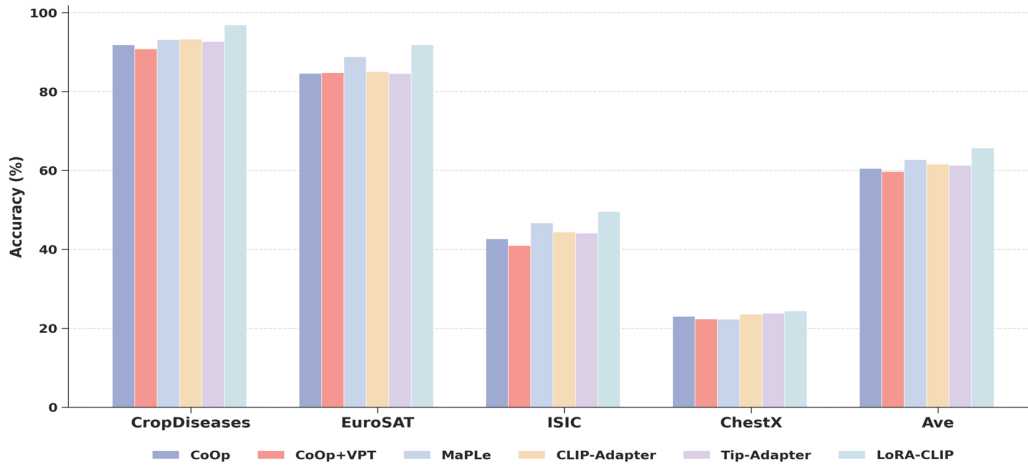


Graphical Abstract

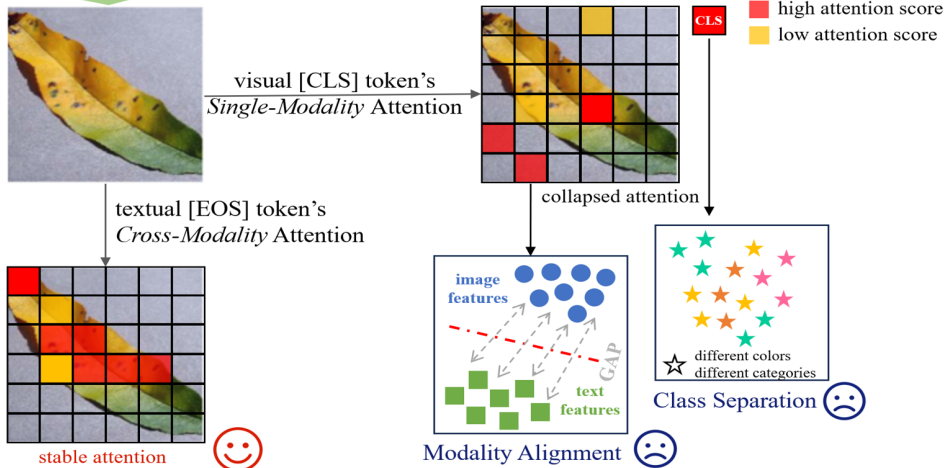
Reviving In-domain Fine-tuning Methods for Source-Free Cross-domain Few-shot Learning

Yaze Zhao, Yicong Liu, Yixiong Zou, Yuhua Li, Ruixuan Li



(a) 5-way 5-shot Accuracy vs. Fine-tuning Methods

A leaf with Peach Bacterial spot is typically yellowish-green and circular with a water-soaked appearance.



(b) Textual [EOS] token shows more stable attention due to the class-related information in texts.

Cross-Domain Few-Shot Learning (CDFSL) aims to adapt large-scale pretrained models to specialized target domains with limited samples, yet the few-shot fine-tuning of vision-language models like CLIP remains underexplored. By establishing multiple fine-tuning baselines of CLIP for CDFSL, we find adapter-based methods (e.g., LoRA) consistently outperform prompt-based ones (e.g., MaPLE)—contrary to in-domain scenarios. To make those effective in-domain methods competitive again in CDFSL, we analyze this phenomenon and discover LoRA's superiority stems from rectifying the collapsed attention of visual [CLS] token, enhancing modality alignment and class separation by focusing on text-related visual regions. Further, we find textual [EOS] token exhibit much better attention to visual samples, and CLIP's standard contrastive loss weakly constrains modality alignment. Based on these insights, we propose Semantic Probe, a plug-and-play attention rectification framework for both adapter- and prompt-based methods. Extensive experiments on four CDFSL benchmarks validate our rationale, achieving state-of-the-art performance and benefiting both fine-tuning paradigms.

Highlights

Reviving In-domain Fine-tuning Methods for Source-Free Cross-domain Few-shot Learning

Yaze Zhao, Yicong Liu, Yixiong Zou, Yuhua Li, Ruixuan Li

- We first establish multiple CLIP fine-tuning baselines for source-free cross-domain few-shot learning (SF-CDFSL), and discover a performance reversal that adapter-based methods (e.g., LoRA) outperform prompt-based ones (e.g., MaPLe), which is contrary to in-domain scenarios.
- We reveal that the performance reversal stems from the attention collapse of the visual token, which causes severe modality misalignment and poor class separation; meanwhile, the textual token shows more stable and discriminative attention to visual regions.
- We propose a plug-and-play Semantic Probe framework consisting of an EOS-guided Attention Rectification (EAR) module and a dynamic Balanced Alignment and Separation (BAS) loss, which revives in-domain fine-tuning methods and achieves state-of-the-art performance on four CDFSL benchmarks.

Reviving In-domain Fine-tuning Methods for Source-Free Cross-domain Few-shot Learning

Yaze Zhao¹, Yicong Liu¹, Yixiong Zou*, Yuhua Li and Ruixuan Li

School of Computer Science and Technology, Huazhong University of Science and Technology, 1037 Luoyu Road, Wuhan, 430070, Hubei, China

ARTICLE INFO

Keywords:
Cross-Domain Few-Shot Learning
Attention Collapse
Modality Gap

ABSTRACT

Cross-Domain Few-Shot Learning (CDFSL) aims to adapt large-scale pretrained models to specialized target domains with limited samples, yet the few-shot fine-tuning of vision-language models like CLIP remains underexplored. By establishing multiple fine-tuning baselines of CLIP for CDFSL, we find adapter-based methods (e.g., LoRA) consistently outperform prompt-based ones (e.g., MaPLe)—contrary to in-domain scenarios. To make those effective in-domain methods competitive again in CDFSL, we analyze this phenomenon and discover LoRA’s superiority stems from rectifying the collapsed attention of visual [CLS] token, enhancing modality alignment and class separation by focusing on text-related visual regions. Further, we find textual [EOS] token exhibit much better attention to visual samples, and CLIP’s standard contrastive loss weakly constrains modality alignment. Based on these insights, we propose Semantic Probe, a plug-and-play attention rectification framework for both adapter- and prompt-based methods. Extensive experiments on four CDFSL benchmarks validate our rationale, achieving state-of-the-art performance and benefiting both fine-tuning paradigms. Codes will be released.

1. Introduction

The past decade has seen significant progress in computer vision [2, 38]. However, this success relies heavily on large-scale, well-annotated datasets like ImageNet, which are widely available in general domains. In contrast, specialized real-world applications, such as medical diagnosis and remote sensing, often face severe data scarcity. The high cost of expert annotations, coupled with stringent privacy and security constraints, typically limits labeled samples to only a few per class, creating significant challenges for deploying robust AI models in these critical domains. Consequently, Cross-Domain Few-Shot Learning (CDFSL) [7, 49, 46] has emerged as a critical paradigm to tackle this. It aims to transfer models pretrained on large-scale general datasets to downstream cross-domain expert datasets where only scarce training samples are available. With the increasing adoption of large pretrained models, source-free fine-tuning [39, 35, 36] of such models has become a critical concern for CDFSL. However, vision-language models exemplified by CLIP [26], which have been extensively applied in various vision tasks due to their remarkable generalizability, remain relatively underexplored for the downstream few-shot fine-tuning in CDFSL tasks.

To address this issue, we first establish multiple downstream few-shot fine-tuning baselines of CLIP by implementing different state-of-the-art methods, including prompt-based tuning [45, 14, 15], and adapter-based tuning [5, 42, 40] for CLIP, as shown in Fig. 1a. However, prior studies [16]

have shown that prompt-based methods typically outperform adapter-based methods in in-domain tasks, whereas in downstream cross-domain scenarios, we find that the adapter-based methods inversely show much higher performance than prompt-based ones, with LoRA-CLIP consistently showing the highest performance. This phenomenon indicates that the few-shot fine-tuning for cross-domain scenarios may exhibit different mechanisms compared with in-domain ones, which have been seldom studied.

To delve into this phenomenon, in this paper, we choose LoRA-CLIP and MaPLe as two top-performing methods from Fig. 1a for an in-depth analysis. Given models fine-tuned with these methods, we first measure the feature distribution of text (augmented with LLM-generated [25] prompt expansions) and visual modalities, and we find LoRA-CLIP’s modality alignment and class separation are much better than those of MaPLe.

To take a closer look at this phenomenon, we then visualize the attention map of visual features. Since AttnTemp [48] noticed the attention collapse problem in directly transferring attention maps to target domains, we find that during the few-shot fine-tuning, MaPLe struggles to rectify the collapse problem compared with LoRA-CLIP, where the visual [CLS] token predominantly focuses on itself, causing the observed modality misalignment and insufficient class separation phenomenon in Fig. 1b. In other words, the model can hardly be fine-tuned to focus on the correct visual regions corresponding to the given class-related text, leading to the modality misalignment and bad class separation of visual samples, which finally causes the performance gap.

To rectify attention collapse, we move beyond the structural parameter modifications of LoRA and seek to harness the efficacy of in-domain fine-tuning methods for CDFSL scenarios. Our observations reveal that the textual [EOS] token exhibits superior cross-attention toward class-relevant

*Corresponding author

✉ zyaz@hust.edu.cn (Y. Zhao); lyc.hust@foxmail.com (Y. Liu);
yixiong@hust.edu.cn (Y. Zou); idcliyuhua@hust.edu.cn (Y. Li);
rxli@hust.edu.cn (R. Li)

ORCID(s): 0009-0000-8810-8929 (Y. Zhao); 0009-0003-9402-503X (Y. Liu); 0000-0002-2125-9041 (Y. Zou); 0000-0002-1846-4941 (Y. Li); 0000-0002-7791-5511 (R. Li)

¹These authors contributed equally to this work.

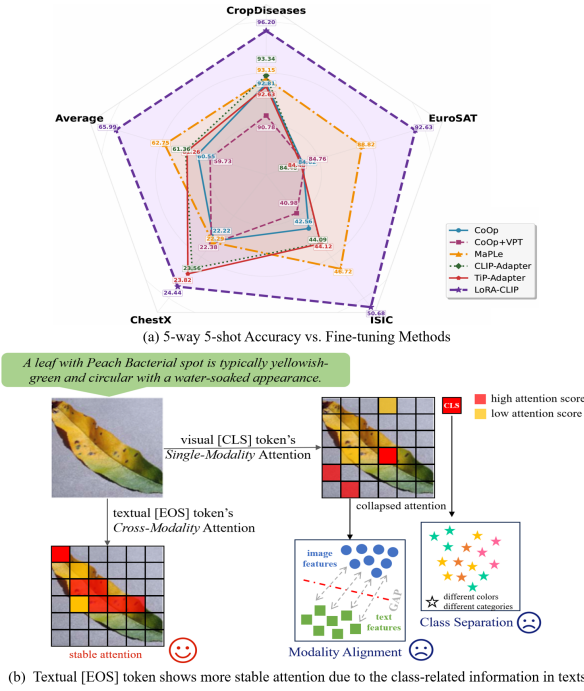


Figure 1: (a) Among these fine-tuning methods, we find LoRA’s performance in the CDFSL task is consistently higher than that of others, which is opposite to the in-domain scenarios. (b) To understand this reversal, we uncover that the cause lies in the collapsed visual attention on cross-domain samples, preventing the model from focusing on visual regions relevant to the given class-related text, while LoRA can better handle than other methods. Based on this, we further find that the EOS token of texts inherently maintains more stable attention on discriminative image areas, which inspires us to develop an EOS-guided attention rectification mechanism that can be plugged into both adapter- and prompt-based fine-tuning, making the latter competitive again in CDFSL.

visual regions, acting as a *semantic oracle* to steer the visual [CLS] token’s focus without requiring extensive parameter updates. Moreover, we also find that CLIP’s standard InfoNCE loss primarily enforces class separation yet provides weak constraints for modality alignment, consistent with the observations in [19] and [30]. Therefore, we propose a novel Semantic Probe framework, which comprises two synergistic components: (1) an EOS-guided Attention Rectification (EAR) module to correct attention maps for better capturing the visual patterns corresponding to class-related texts, and (2) a dynamic Balanced Alignment and Separation (BAS) loss to enhance the learning of modality alignment and class separation.

In summary, our contribution can be listed as:

- By establishing multiple fine-tuning baselines of CLIP on the CDFSL task, we are the first to find the performance gap between adapter-based and prompt-based methods, opposite to the in-domain scenarios.

- We delve into this phenomenon for interpretation and find that the reason lies in the difference in the fine-tuning of attention networks, which causes the modality misalignment and poor class separation problem, and finally leads to the performance gap.
- Based on the interpretation, we further propose a Semantic Probe framework, which includes an EAR module to improve the fine-tuning of attention networks, and a BAS module to enhance the learning of both modality alignment and class separation.
- Extensive experiments on four widely used CDFSL datasets and various fine-tuning methods show that our method consistently improves performance and outperforms state-of-the-arts works.

2. Why Does LoRA Show Better Fine-tuning Results in the CDFSL Task?

Due to the top performance shown in Fig. 1a, we select LoRA-CLIP [10, 40] and MaPLe [15] as the representative adapter-based and prompt-based methods, respectively.

2.1. Preliminaries

Cross-Domain Few-Shot Learning (CDFSL) involves adapting a model to a target dataset $D_T = \{(x_i^T, y_i^T)\}_{i=1}^{N_T}$, where only scarce data is available, after pretraining it on a source dataset $D_S = \{(x_i^S, y_i^S)\}_{i=1}^{N_S}$, which contains abundant labeled samples. Typically, target datasets have large distribution differences from general domains, such as medical imaging or satellite imagery. CDFSL approaches commonly follow the N -way K -shot paradigm to construct episodes (i.e., small datasets) from D_T . Each episode consists of a support set, denoted as $S = \{(x_{ij}, y_i)\}_{i=1, j=1}^{N, K}$, with N classes and K samples per class for training, and a disjoint query set, denoted as $Q = \{(x_{iq}, y_i)\}_{i=1, q=1}^{N, M}$, $S \cap Q = \emptyset$, for evaluating performance on these N classes.

CLIP introduces a contrastive learning framework to align visual and textual modalities. For each image-text pair (x_i^v, x_i^t) , CLIP employs two independent encoders to extract features, $v_i = f_v(x_i^v)$ and $t_i = f_t(x_i^t)$, trained using a symmetric contrastive loss over a batch of B positive pairs:

$$L_{\text{clip}} = \frac{L_{i \rightarrow t} + L_{t \rightarrow i}}{2} \quad (1)$$

MaPLe is the first multi-modal prompt-tuning method designed for CLIP. It jointly updates textual and visual prompts across layers via a vision–language coupling function. At each transformer layer j ($0 \leq j < L$), the updates are defined as:

$$\begin{aligned} [P_j, W_j] &= T_j(P_{j-1}, W_{j-1}) \\ [c_j, E_j, \tilde{P}_j] &= V_j([c_{j-1}, E_{j-1}, F_{j-1}(P_{j-1})]) \end{aligned} \quad (2)$$

where P represents the textual prompt tokens, W and E denote the textual and visual input tokens, respectively, T

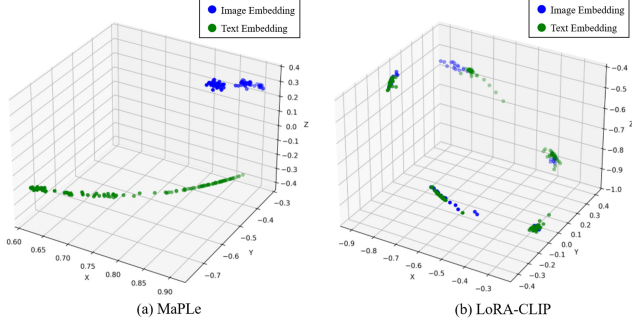


Figure 2: DOSNES visualization of embeddings of MaPLe and LoRA-CLIP. LoRA-CLIP (right) yields a smaller modality gap and tighter clusters.

and V are the text and image encoders, F is the vision-language coupling function, and c is the visual class token.

LoRA is an adapter-based reparameterization tuning approach [12] that enhances the efficiency of fine-tuning large-scale models by injecting low-rank matrices into the attention layers of transformer architectures. Specifically, it modifies the weight matrices of the attention mechanism by adding low-rank updates (A_* , B_*), which significantly reduce the number of trainable parameters while introducing no additional inference latency. The updates are applied as follows:

$$\begin{aligned} W'_q &= W_q + \Delta W_q = W_q + A_q B_q \\ W'_k &= W_k + \Delta W_k = W_k + A_k B_k \\ W'_v &= W_v + \Delta W_v = W_v + A_v B_v \end{aligned} \quad (3)$$

Additionally, to align with CLIP's pre-training paradigm and enrich textual modality information [27], we select 30 descriptions per support set class as textual prompts during the fine-tuning phase of each episode. The class-wise mean of text features is used as weights for the text classifier. Further details are provided in Section D.

2.2. CLIP suffers from modality gap and insufficient class separation under CDFSL

To investigate this performance gap, we first visualize the feature distributions of both image features (blue) and text features (green) extracted by LoRA-CLIP and MaPLe on the target domain, using DOSNES [21] projection, as shown in Fig. 2. Our key observations reveal that: In cross-domain scenarios, (1) MaPLe exhibits pronounced modality gap between visual and textual features, with poor class separation; whereas (2) LoRA-CLIP projects both visual and textual features with less modality separation, while maintaining well-separated clusters.

Fig. 3 illustrates the distribution of class features by the T-SNE visualization. The text modality includes 30 text features and one class mean feature (marked with \star) for each class, while image features are represented by \circ , with different classes distinguished by different colors. In comparison to MaPLe, LoRA-CLIP demonstrates superior

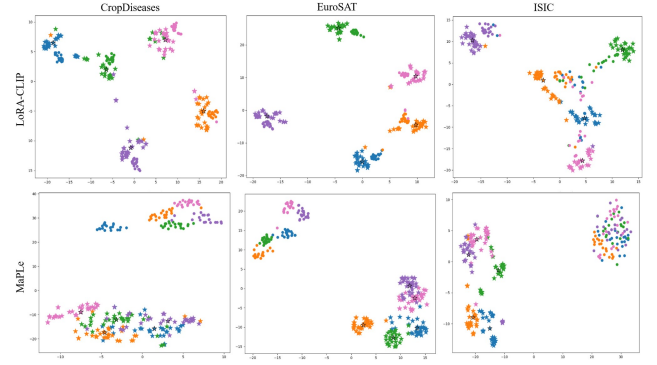


Figure 3: T-SNE visualization of the embeddings of LoRA-CLIP and MaPLe. The former (top row) achieves clearer class boundaries for both visual and textual features.

class separability, which is advantageous for classification tasks.

To further quantitatively validate our observations, we employ the *align_score* [3] and *modality_gap* [19] to assess modality alignment, alongside the Calinski-Harabasz (CH) Index to evaluate class separability. The *align_score* is defined as follows:

$$align_score = \frac{1}{U \times |S|} \sum_{i \in (0, N)} e_i^v \cdot e_i^t \quad (4)$$

where e^v represents image features, e^t represents the text features corresponding to the true class, U (i.e., 30) denotes the number of textual prompts per class, $|S| = N \times K$ is the size of the support set, and N is the number of classes.

The *modality_gap* quantifies the Euclidean distance between the mean vectors of image and text features, defined as:

$$modality_gap = \left\| \frac{1}{|S|} \sum_{i=1}^{|S|} e_i^v - \frac{1}{N_t} \sum_{i=1}^{N_t} e_i^t \right\|_2 \quad (5)$$

where $N_t = N \times U$ is the total number of text prompts across all classes.

The CH Index evaluates the ratio of inter-class compactness to intra-class separation, calculated as:

$$CH(X, L) = \frac{B(X, L) \cdot (n_{samples} - n_{labels})}{W(X, L) \cdot (n_{labels} - 1)} \quad (6)$$

where X represents the feature matrix, containing $n_{samples}$ data points, L represents the cluster labels, containing n_{labels} categories, $B(X, L)$ represents the between-cluster dispersion, and $W(X, L)$ denotes the within-cluster dispersion. A higher CH index value indicates greater class separation.

Fig. 4(a,b) shows the modality alignment metrics from the final layer outputs of LoRA-CLIP and MaPLe across training epochs. In Fig. 4a, the *align_score* (higher values indicate better alignment) demonstrates that LoRA-CLIP consistently outperforms MaPLe. Similarly, Fig. 4b illustrates the *modality_gap* (lower values are preferable), where LoRA-CLIP achieves a substantially smaller gap compared

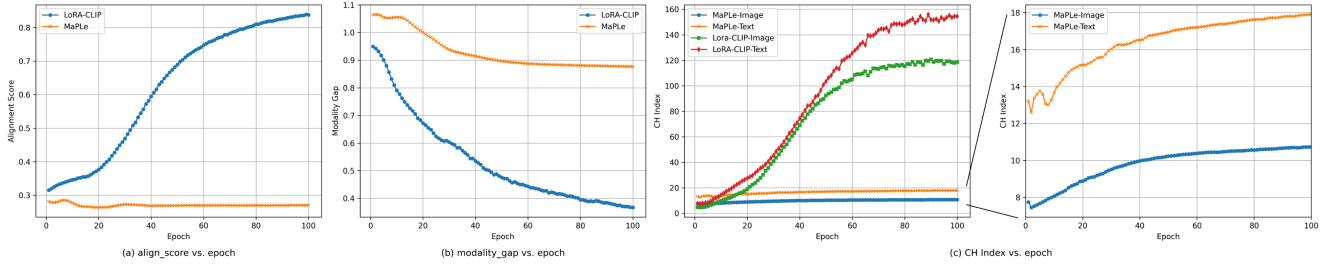


Figure 4: The modality alignment and class separation metrics of the last-layer features evolve with training epochs for both LoRA-CLIP and MaPLE: (a) align_score (higher is better). (b) modality_gap (lower is better). (c) Calinski-Harabasz Index (higher is better). LoRA-CLIP is more effective than MaPLE at optimizing both modality alignment and class separation during fine-tuning for CDFSL tasks.

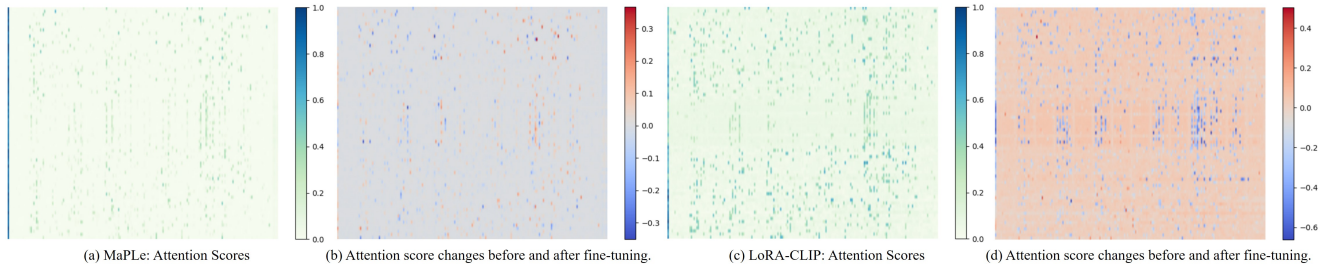


Figure 5: Attention scores of the CLS token on image tokens and the changes after fine-tuning. Before fine-tuning, the CLS token exhibits severe self-attention and neglects informative regions. LoRA markedly shifts attention toward class-relevant patches after fine-tuning, while MaPLE yields almost no change.

to MaPLE. Fig. 4c depicts the CH Index for both visual and textual features over training epochs, revealing an increasing trend for both models, with LoRA-CLIP converging to a significantly higher value than MaPLE, indicating superior class separability.

In summary, the above results demonstrate that **LoRA-CLIP consistently outperforms MaPLE in both modality alignment and class separation for CDFSL tasks**, which are closely related to their performance disparities.

2.3. Collapsed attention under CDFSL leads to modality gap and insufficient class separation

Since [48] pointed out that the attention *directly transferred* to cross domains (especially distant domains) tends to collapse (focusing solely on the CLS token), we are inspired to analyze the attention distribution of the visual CLS token under CLIP to understand modality gap and class separation issues. As shown in Fig. 5, the Y-axis corresponds to the batch dimension, and the X-axis represents the token positions within each sample. Fig. 5a shows the heatmap of the CLS token’s attention distribution over image tokens, with Fig. 5b depicting changes in CLS token’s attention scores before and after fine-tuning. Fig. 5c and Fig. 5d present the corresponding attention heatmaps for LoRA-CLIP arranged in the same order.

Fig.5 highlights two key findings in the visual features:

- **Attention Collapse:** An attention collapse problem exists widely, consistent with [48], where the CLS token predominantly focuses on itself across samples, as seen in

the high attention scores in the leftmost columns of Fig. 5a and Fig. 5c.

- **LoRA-CLIP vs. MaPLE:** MaPLE struggles to address the attention collapse issue, as shown in Fig. 5b, where most attention scores remain unchanged (gray means zero change) after the cross-domain fine-tuning, and the major attention is still on the CLS token in Fig. 5a. Conversely, Fig. 5d demonstrates that LoRA can effectively adjust the attention scores during fine-tuning, resulting in diverse focus across various local patch tokens in Fig. 5c.

Therefore, we hold that this inconsistency in attention distribution leads to both the modality gap and the poor class separation problem:

- **Modality Misalignment:** Given the text that describes the visual clues in the image, if the visual CLS token fails to focus on the corresponding regions of the image, the visual feature can hardly match the text feature, leading to modality misalignment and gap.

- **Poor Class Separation:** If the CLS token can’t focus on discriminative patches in the image, the discriminability of the visual feature will also be harmed, leading to poor class separation.

Based on the above observations, we can explain the superiority of LoRA over other fine-tuning methods in cross-domain scenarios as follows: LoRA directly modifies the parameter matrices (i.e., the $Q/K/V$ parameters) involved in the attention mechanism, enabling a more effective correction of the collapsed attention. This, in turn, helps mitigate the resulting issues of modality misalignment and poor class

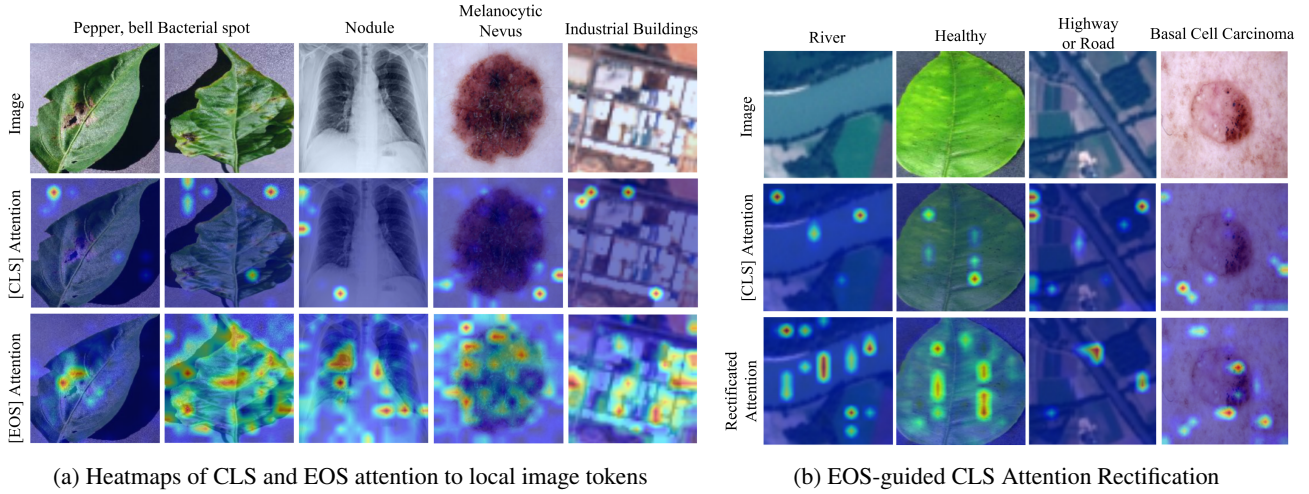


Figure 6: (a) Heatmaps of the visual CLS and textual EOS token’s attention to image. The EOS token demonstrates significantly stronger capability in capturing visual semantic information compared to the CLS token. (b) EOS-guided CLS Attention Rectification.

separation, thereby significantly improving CLIP’s performance in CDFSL tasks.

2.4. Inspiration: addressing attention collapse by introducing text information

Since we verified that the rectification of collapsed attention is the core of effective few-shot fine-tuning in the CDFSL problem, a question naturally arises: *Can we use another way (other than LoRA) to help the attention rectification to better utilize those advantageous in-domain fine-tuning methods in CDFSL?* Given the text modality, we ask: can we take the text information to improve the rectification? While current work [48] merely focuses on the CLS token’s attention in solely the visual branch, the text modality actually provides prior knowledge about what the vision network should focus on, potentially guiding the calibration of the CLS token’s attention.

For example, when reading an unfamiliar article, we may easily overlook important information in this article, just like how the visual CLS token misses critical regions of the image in cross-domain scenarios. However, if an oracle provides us with the information about what to focus on (such as finding the birthday of someone), it will be easier for us to capture the relevant details. In this context, the text modality essentially serves as the oracle, directing the vision network to relevant regions and aiding attention rectification.

To validate this intuition, we further visualize the heatmaps of the CLS token and the textual EOS token’s attention to local patch tokens in Fig.6a. We find that the EOS token consistently focuses on more accurate and comprehensive discriminative regions compared with the visual CLS token, which verifies our intuition and motivates us to leverage the EOS token to enhance attention rectification in CLIP for CDFSL tasks. Based on this intuition, we can further enhance the attention rectification beyond LoRA, reviving those in-domain fine-tuning methods for CDFSL.

3. Methods

Based on the above interpretation and analysis, we aim to address the attention collapse problem and improve both the modality alignment and class separation. To address these issues, we propose the Semantic Probe framework, which consists of two synergistic components: (1) an EOS-guided Attention Rectification (EAR) module to correct attention maps; and (2) a Balanced Alignment and Separation (BAS) loss to dynamically enhance the learning of both the modality alignment and class separation, as illustrated in Fig.7a.

3.1. EOS-guided Attention Rectification

To correct the attention bias of the visual CLS token in CLIP, we aim to enhance its focus on semantically informative image tokens. These tokens can be identified using the textual EOS token’s attention, which inherently captures richer class-specific information. As shown in Fig. 6b, when the EOS attention matrix is used to refine the CLS attention, the CLS token exhibits improved focus on relevant image regions and becomes more aligned with texts.

Building upon this, we propose an EOS-guided Attention Rectification module (Fig. 7b). For the i -th layer in CLIP, the attention weights of the CLS token with respect to all visual tokens are defined as:

$$Attention_i^{cls} = softmax\left(\frac{v^{cls} \cdot W_q(v \cdot W_k)^T}{\sqrt{d_v}}\right) \in \mathbb{R}^{1 \times (1+n)} \quad (7)$$

Here, $v^{cls} = v[0] \in \mathbb{R}^{d_v}$ represents the global CLS token, $v \in \mathbb{R}^{(1+n) \times d_v}$ denotes the sequence of visual tokens input to this layer (including both the CLS token and image patch tokens), and $W_q, W_k \in \mathbb{R}^{d_v \times d_v}$ are the learnable Query and Key transformation matrices, respectively.

Concurrently, we compute the attention matrix of the textual EOS token over the n image patch tokens:

$$Attention_i^{eos} = softmax\left(\frac{(t^{eos} \cdot E) \cdot W'_q(v[1:] \cdot W'_k)^T}{\sqrt{d_v}}\right) \quad (8)$$

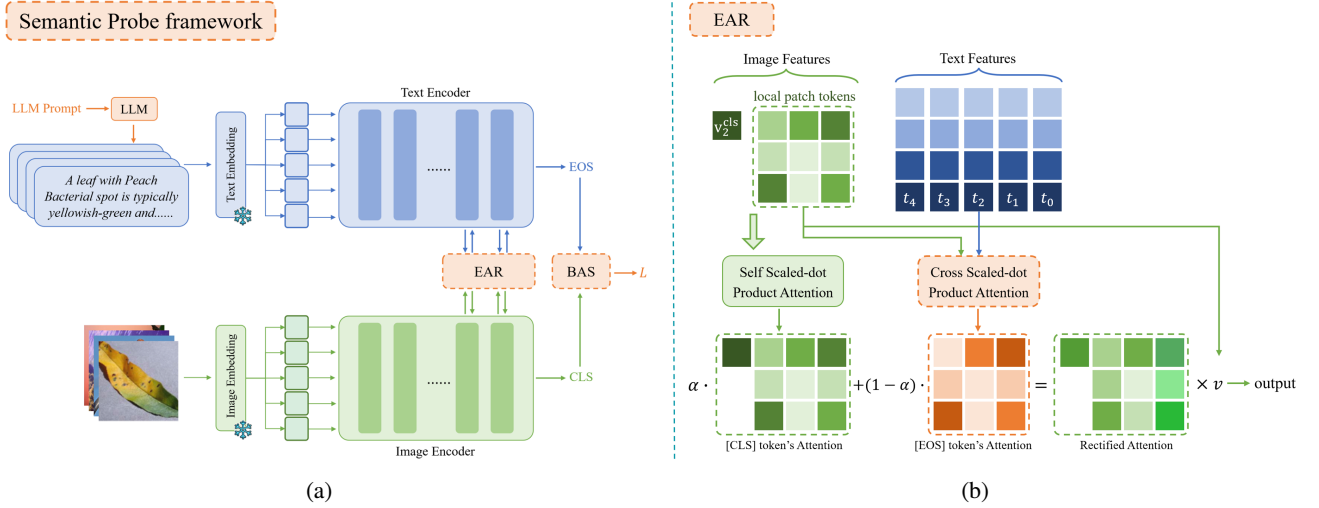


Figure 7: (a) Overview of our Semantic Probe framework, which revives in-domain fine-tuning methods for CDFSL. The EOS-guided Attention Rectification module is plugged to the final layers of CLIP to rectify attention, while the Balanced Alignment and Separation loss replaces the original contrastive loss to dynamically guide the model's focus between modality alignment and class separation. (b) EAR module. The attention matrix from the EOS token to visual features is used to rectify the attention of the CLS token. Through weighted summation, EAR reduces the CLS token's excessive self-focus and redirects its attention toward discriminative visual tokens.

In this equation, $t^{eos} \in \mathbb{R}^{d_t}$ represents the textual EOS token obtained from the i -th layer of CLIP's text encoder, $v[1:] \in \mathbb{R}^{n \times d_v}$ specifically refers to the sequence of image patch tokens, excluding the visual CLS token, as our focus is on the EOS token's attention to the content regions of the image. Due to the inherent dimensional discrepancy between visual and textual embeddings, the E matrix is designed with dimensions $\mathbb{R}^{d_t \times d_v}$ to project the textual EOS token into the visual feature space, enabling effective cross-modal interaction.

Subsequently, we calculate the rectified attention distribution matrix by performing a weighted summation of the above two attention matrices:

$$Attention_i^{cls'} = \alpha \cdot Attention_i^{cls} + (1 - \alpha) \cdot [0; Attention_i^{eos}] \quad (9)$$

where α is a coefficient with a value less than 1. After multiplying $Attention_i^{cls}$ by α , we effectively reduce the CLS token's self-attention score, thereby suppressing its tendency for excessive self-focus. As demonstrated in Section 2.3, the attention scores for image tokens within $Attention_i^{eos} \in \mathbb{R}^{1 \times n}$ are typically higher than their corresponding values in $Attention_i^{cls}$. Consequently, this weighted summation increases the attention scores directed towards the image tokens, guiding the global CLS token to concentrate more on discriminative, category-relevant visual information. It is important to note that since both attention distributions are normalized via the softmax function (i.e., $\sum Attention_i^{eos} = \sum Attention_i^{cls} = 1$), their weighted sum also remains normalized, ensuring the stability of the feature distribution. In practice, to achieve dimension alignment, we pad a zero before the elements of $Attention_i^{eos}$, making its dimension consistent with $Attention_i^{cls}$.

Finally, the rectified CLS token feature at the current layer, f_i^{cls} , is obtained by multiplying the $Attention_i^{cls'}$ $\in \mathbb{R}^{1 \times (1+n)}$ with the Value-transformed visual tokens:

$$f_i^{cls} = Attention_i^{cls'} \cdot (v \cdot W_v) \in \mathbb{R}^{d_v} \quad (10)$$

3.2. Balanced Alignment and Separation

As observed in Fig. 4 and Fig. 12 in Appendix, while both modality alignment and class separation improve during training, their simultaneous optimization can lead to an imbalanced learning of either side. To further enhance both criteria, we propose a strategy that balances these two critical objectives.

Specifically, existing methods adopt only a one-way image-to-text contrastive loss. As an initial enhancement, we first incorporate the complete bidirectional contrastive loss as defined in Eqs. (1), (14), (15), which serves as our primary loss term:

$$L_1 = L_{clip} \quad (11)$$

To directly constrain modality alignment, we introduce a secondary loss term, L_2 , formulated as the harmonic mean of *align_score* and *modality_gap*:

$$L_2 = \frac{2 \times (1 - align_score) \times modality_gap}{(1 - align_score) + modality_gap} \quad (12)$$

Subsequently, we propose a balanced optimization strategy — Balanced Alignment and Separation (BAS). Unlike static weighting, BAS adaptively adjusts the contribution of each loss term based on their real-time batch-wise values. The adjustment is achieved through a dynamic weighting coefficient, which is determined by the current value of L_2 :

$$\beta = \frac{w}{1 + e^{-k(L_2 - T)}}, \quad L_{BAS} = L_1 + \beta \cdot L_2 \quad (13)$$

Table 1

Accuracies (%) of target domain datasets of 5-way 1-shot and 5-shot tasks. * denotes that data augmentation was utilized in our implementation. Refer to the Appendix for the extended table.

Task	Method	Mark	backbone	ISIC	ChestX	EuroSAT	CropDisease	Avg
5-way 1-shot	StepSPT [36]	TPAMI-25	ViT/CLIP	32.97	22.84	70.01	84.84	52.66
	Tip-Adapter* [43]	ECCV-22	ViT/CLIP	32.68	22.24	75.44	77.15	51.87
	AMU-Tuning* [28]	CVPR-24	ViT/CLIP	32.29	21.56	72.24	80.20	51.57
	LP++* [13]	CVPR-24	ViT/CLIP	33.63	21.72	73.05	81.84	52.56
	LDC* [17]	CVPR-25	ViT/CLIP	33.72	22.32	74.39	84.07	53.62
	LoRA-CLIP [40]	CVPR-24	RN50/CLIP	32.01	21.76	57.79	65.24	44.20
	CoOp [45]	IJCV-22	ViT/CLIP	29.47	20.95	68.16	79.27	49.46
	CoOp + OURS	-	ViT/CLIP	29.64	21.33	69.77	80.93	50.42
	CLIP-Adapter [5]	IJCV-24	ViT/CLIP	31.31	21.51	67.83	81.14	50.44
	CLIP-Adapter + OURS	-	ViT/CLIP	32.83	22.73	70.19	82.03	51.94
	Tip-Adapter [43]	ECCV-22	ViT/CLIP	30.36	21.96	72.05	76.55	50.23
	Tip-Adapter + OURS	-	ViT/CLIP	31.88	22.23	74.29	78.19	51.65
	Maple [15]	CVPR-23	ViT/CLIP	31.10	20.89	75.66	81.87	53.04
	Maple + OURS	-	ViT/CLIP	34.27	21.41	82.94	82.83	55.36
	LoRA-CLIP [40]	CVPR-24	ViT/CLIP	34.45	21.73	80.34	84.95	55.37
LoRA-CLIP + OURS	-	ViT/CLIP	38.77	23.65	82.94	85.11	57.62	
5-way 5-shot	StepSPT [36]	TPAMI-25	ViT/CLIP	52.12	26.36	89.40	96.01	65.97
	Tip-Adapter* [43]	ECCV-22	ViT/CLIP	46.96	24.07	87.24	94.19	63.12
	AMU-Tuning* [28]	CVPR-24	ViT/CLIP	44.60	23.34	88.47	94.26	62.66
	LP++* [13]	CVPR-24	ViT/CLIP	48.49	23.89	87.48	94.47	63.58
	LDC* [17]	CVPR-25	ViT/CLIP	49.70	25.89	90.82	96.71	65.78
	LoRA-CLIP [40]	CVPR-24	RN50/CLIP	46.53	23.00	77.26	87.42	58.55
	CoOp [45]	IJCV-22	ViT/CLIP	42.56	22.22	84.62	92.81	60.55
	CoOp + OURS	-	ViT/CLIP	43.32	22.68	85.77	94.29	61.52
	CLIP-Adapter [5]	IJCV-24	ViT/CLIP	44.09	23.56	84.48	93.34	61.36
	CLIP-Adapter + OURS	-	ViT/CLIP	44.91	23.73	85.37	93.00	61.75
	Tip-Adapter [43]	ECCV-22	ViT/CLIP	44.12	23.82	84.48	92.63	61.26
	Tip-Adapter + OURS	-	ViT/CLIP	45.63	24.49	85.91	93.75	62.44
	Maple [15]	CVPR-23	ViT/CLIP	46.72	22.29	88.82	93.15	62.75
	Maple + OURS	-	ViT/CLIP	53.11	24.86	92.50	94.85	66.33
	LoRA-CLIP [40]	CVPR-24	ViT/CLIP	50.68	24.44	92.63	96.20	65.99
LoRA-CLIP + OURS	-	ViT/CLIP	55.95	25.79	93.43	96.88	68.01	

Here, β is the sigmoid-shaped weighting coefficient. w sets the maximum initial value of β , k controls the steepness of the decay, and T defines the threshold of L_2 at which the decay becomes significant. When L_2 is high (indicating poor modality alignment), β approaches w , giving more weight to L_2 and emphasizing modality alignment. As L_2 decreases and falls below the threshold T , β sharply drops, effectively reducing the influence of L_2 and prompting the model to primarily focus on class separation (driven by L_1).

During inference, the image is assigned to the class whose text embedding yields the highest cosine similarity with the visual feature.

4. Experiments

4.1. Dataset and Implementation Details

We fine-tuning and evaluate CDFSL performance on four target-domain datasets from the BSCD-FSL benchmark [7]: CropDiseases [23], EuroSAT [9], ISIC2018 [1], and ChestX [33]. We adopt the ViT-Base/16 network as the backbone for all experiments. Fine-tuning was performed for a total of 100 epochs. Evaluation was consistently conducted 400 times under both the 5-way 1-shot and 5-way 5-shot settings, with the mean classification accuracy reported for

all results. The parameter α in Eq. (9) and the parameters w , k and T in Eq. (13) are set to 0.8 and 7, 5, 3.5, respectively. See detailed hyperparameter experiments in the Appendix Section E. All experiments were conducted on a single NVIDIA RTX 4090 GPU.

4.2. Comparison with State-of-the-Art Methods

For the SF-CDFSL [36] benchmark setting, we reproduce multiple fine-tuning methods tailored for CLIP, following the experimental protocols exactly as specified in their original studies. These competing approaches span representative technical paradigms in PEFT of vision-language models, including prompt learning (CoOp) in the text branch, adapter-based methods (CLIP-Adapter, Tip-Adapter, LoRA-CLIP), and multi-modal prompt learning (Maple)—as well as recent advanced tuning strategies (AMU-Tuning, LP++, LDC, StepSPT). As presented in Tab. 1, our Semantic Probe framework consistently enhances the performance of all baseline methods.

4.3. Ablation Study

The effects of each component. Tab. 2 presents ablation results for the 5-way 5-shot classification task, evaluating

Table 2

Ablation study of the 5-way 5-shot task under MaPLe and LoRA-CLIP (LP denotes using prompts generated by LLM).

Method	LP	BAS	EAR	ChestX	ISIC	EuroSAT	CropDiseases	Ave.
MaPLe				22.29	46.72	88.82	93.15	62.75
	✓			23.62	49.02	89.58	93.00	63.81
	✓	✓		24.10	51.70	91.77	94.13	65.43
	✓		✓	23.70	50.96	91.99	94.58	65.31
	✓	✓	✓	24.86	53.11	92.50	94.85	66.33
LoRA-CLIP				24.44	50.68	92.63	96.20	65.99
	✓			24.86	54.55	92.78	96.22	67.10
	✓	✓		25.21	55.14	93.10	96.56	67.50
	✓		✓	25.30	55.79	93.13	96.71	67.73
	✓	✓	✓	25.79	55.95	93.43	96.88	68.01

Table 3

Comparison of different fixed β values for the 5-way 1-shot classification task.

β	ChestX	ISIC	EuroSAT	CropDiseases	Ave.
0	21.90	38.82	82.96	84.60	57.07
0.2	22.00	39.32	82.50	84.05	56.97
0.4	22.01	39.26	81.89	83.98	56.79
0.6	21.92	39.20	82.25	84.23	56.90
0.8	21.86	39.05	82.74	84.22	56.97
0.9	21.88	38.99	82.89	84.23	57.00
Ours	22.60	39.61	83.06	84.61	57.47

the EAR and BAS components under MaPLe and LoRA-CLIP methods. For MaPLe, BAS alone improves average accuracy from 63.81% to 65.43%, EAR alone to 65.31%, and their combination achieves 66.33%. Similar improvements are observed with LoRA-CLIP, where the combined EAR and BAS yield the highest performance at 68.01%. These results also confirm that optimizing modality alignment and class separation significantly enhances CLIP’s performance.

A vanilla strategy of β being a selected constant value.

As a comparative study, we evaluate a vanilla strategy where the weighting coefficient β is a fixed constant throughout training, as opposed to our dynamic BAS approach. Tab. 3 presents the results for the 5-way 1-shot classification task (100 episodes) on LoRA-CLIP + Ours. We observe that fixed β values fail to provide some performance gains over the baseline without our modules (i.e., $\beta = 0$), and their performance is highly sensitive to the chosen value. For instance, values like 0.2 and 0.9 yield similar average accuracies, but none of the fixed values can match the performance of our dynamic BAS strategy. This confirms that a static weighting scheme is less effective at managing the intricate trade-off between modality alignment and class separation, which our dynamic loss addresses by adaptively adjusting the optimization focus.

5. Related Work

Cross-Domain Few-Shot Learning (CDFSL) aims to adapt pretrained models to distant target domains (e.g., ISIC2018) using limited samples for rapid generalization. Existing methods can be broadly categorized into two types: meta-learning-based approaches [32, 44], which utilize samples in each episode to enable the model to rapidly adapt to the feature distribution of the target domain; transfer-based methods [18, 48], which concentrate solely on enhancing the

generalization capability of the model during the training phase. We focus on the source-free cross-domain few-shot learning (SF-CDFSL) setting where only the pre-trained model and few-shot target-domain data are accessible.

Parameter-Efficient Fine-Tuning (PEFT) for Vision-Language Models. Current PEFT strategies for VLMs primarily consist of two paradigms: prompt-based methods [45, 15] that inject trainable vectors into text or visual inputs of frozen encoders; and adapter-based methods that inserted bottleneck modules [43, 5] or low-rank matrix [40] to efficiently update model parameters. Despite their success for in-domain fine-tuning, the potential and specific tailoring of these methods for VLM-based SF-CDFSL tasks remain underexplored.

6. Conclusion

In this work, we establish multiple CLIP-based baselines and identify that CLIP suffers from attention collapse in CDFSL. To address this, we introduce a Semantic Probe framework, comprising an EOS-guided Attention Rectification module and a dynamic Balanced Alignment and Separation loss, which collaboratively improve both modality alignment and class separation. Our approach achieves state-of-the-art performance on SF-CDFSL benchmarks.

A. Detailed Dataset Description

Our experimental setup follows the BSCD-FSL [7] benchmark, addressing the challenge of significant distributional shifts across four distinct target domain datasets. Detailed information on these datasets is provided below:

CropDiseases [23] is a dataset including 54,306 images of 14 crop species (Apple, Blueberry, Cherry, Corn, Grape, Orange, Peach, Bell Pepper, Potato, Raspberry, Soybean, Squash, Strawberry, and Tomato) with 26 diseases (or healthy). The samples of this dataset are listed in Fig. 8. CropDiseases images are natural images, but are very specialized (specific to the agriculture industry), so the domain gap here is larger than in the previous cross-domain setting [29].

EuroSAT [9] is a dataset for land use and land cover classification. EuroSAT based on Sentinel-2 satellite imagery, covers 13 spectral bands and consists of 10 categories including Industrial Buildings, Residential Buildings, Annual Crop, Permanent Crop, River, Sea & Lake, Herbaceous Vegetation, Highway, Pasture and Forest, with a total of 27,000 annotated and geographically referenced images. Compared to CropDiseases, EuroSAT images are less similar to *mini*Imagenet (source domain dataset) as they have lost perspective distortion, but are still color images of natural scenes. The samples of this dataset are listed in Fig. 9.

The **ISIC2018** [1] dataset was published by the International Skin Imaging Collaboration (ISIC) as a large-scale dataset of dermoscopy images containing 10,015 images of seven skin injury types (melanoma, melanocytic nevus, basal cell carcinoma, actinic keratosis, benign keratosis,



Figure 8: Samples from CropDiseases.

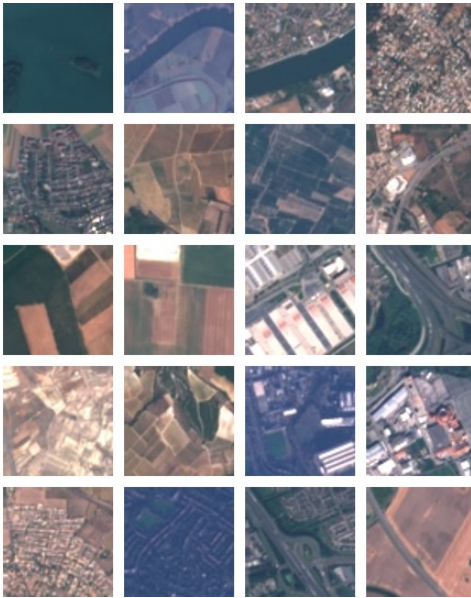


Figure 9: Samples from EuroSAT.

dermatofibroma, or a vascular lesion). ISIC2018 images are even less similar to *miniImagenet* as they have lost perspective distortion and no longer represent natural scenes. The samples of this dataset are listed in Fig. 10.

ChestX-ray14 is the largest lung X-ray database to date, which contains more than 100,000 pre-X-ray views for 14 lung diseases. Categories 1 to 14 correspond to 14 lung diseases, and category 15 indicates no disease. [33] studied the images of eight diseases in this database and constructed the ChestX-ray8 dataset, which comprises 108,948 frontal view X-ray images of 32,717 unique patients with the text-mined eight disease image labels (where each image can have multi-labels) from the associated radiological reports using natural language processing. In this work, we use **ChestX-ray8** for cross-domain testing, consistent with [7].

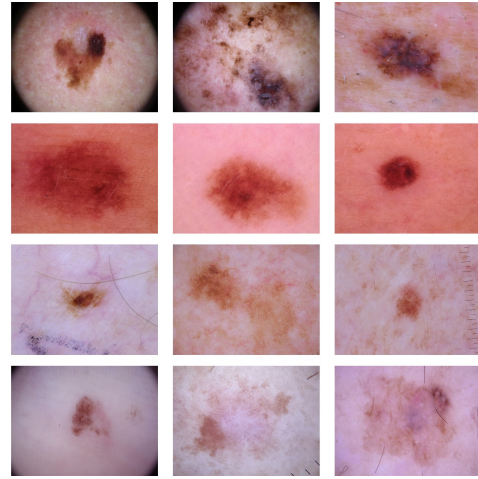


Figure 10: Samples from ISIC2018.

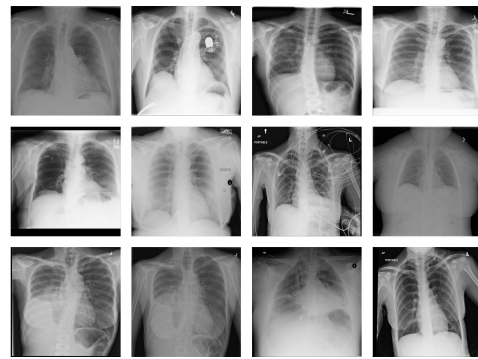


Figure 11: Samples from ChestX.

Table 4

Information Entropy of token attention over image patches.

Dataset	Visual [CLS] token	Textual [EOS] token	Rectified [CLS] token
Ches.	0.6100	0.7887	0.7094
ISIC.	0.7646	0.8758	0.8344
Euro.	0.8182	0.8593	0.8604
Crop.	0.7284	0.8991	0.8055
Ave.	0.7303	0.8557	0.8024

ChestX is the most dissimilar to *miniImagenet* across the four target domains as its images have lost perspective distortion, do not represent natural scenes, and have lost 2 color channels. The samples of this dataset are listed in Fig. 11.

B. Quantitative proof of mitigating attention collapse

In Table 4, we also compute the Mean Normalized Information Entropy of attention distributions over image patches on the full validation set for: (1) raw visual [CLS] token; (2) textual [EOS] token; (3) EAR-rectified [CLS] token. Higher entropy indicates more evenly distributed attention across image patches, reflecting less self-focus and better coverage of discriminative visual regions. After rectification, the average entropy increases to 0.8024, mitigating cross-domain attention collapse.

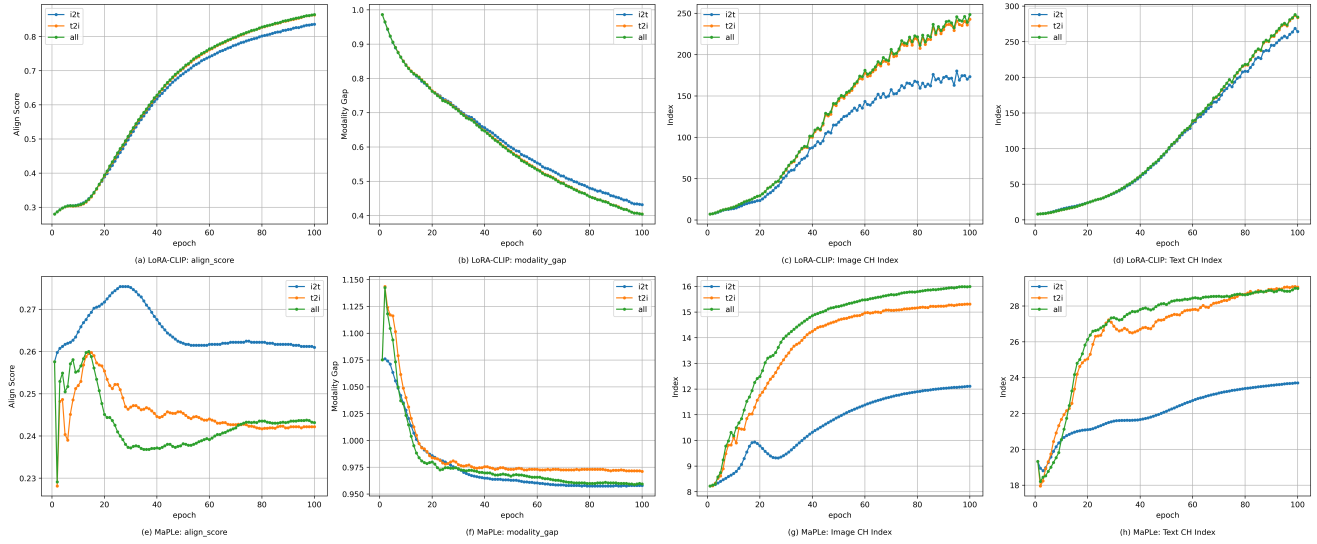


Figure 12: The alignment/aggregation metrics under different losses across training epochs. The modality alignment is only marginally affected by the choice of loss function, whereas the class aggregation improves significantly after the text-to-image term $L_{t \rightarrow i}$ is introduced. This suggests that CLIP’s InfoNCE loss primarily emphasizes class separation, with relatively weak constraints on modality alignment.

C. Contrastive loss lacks constrain to modality alignment but rather class aggregation

To analyse the underlying reasons for the performance gap between LoRA-CLIP and MaPLE, we also examine the role of the original loss function of CLIP. CLIP uses InfoNCE [24] loss to train the model, which consists of two parts:

- Image-to-text contrastive loss:

$$L_{i \rightarrow t} = -\frac{1}{B} \sum_{i=1}^B \log \frac{\exp(\text{sim}(v_i, t_i)/\tau)}{\sum_{j=1}^B \exp(\text{sim}(v_i, t_j)/\tau)} \quad (14)$$

- Text-to-image contrastive loss:

$$L_{t \rightarrow i} = -\frac{1}{B} \sum_{i=1}^B \log \frac{\exp(\text{sim}(t_i, v_i)/\tau)}{\sum_{j=1}^B \exp(\text{sim}(t_i, v_j)/\tau)} \quad (15)$$

where $\text{sim}(a, b) = \frac{a^T b}{\|a\| \|b\|}$ represents cosine similarity, and τ is a temperature parameter.

Existing CDFSL baselines rely solely on the image-to-text contrastive loss term $L_{i \rightarrow t}$ for optimization. Some works like [19] and [30] argue that CLIP’s contrastive loss has minimal impact on guiding modality alignment. This view is supported by Figure 12, which compares the modality alignment metrics of LoRA-CLIP (panels a, b) and MaPLE (panels e, f) under different contrastive loss settings. Notably, when the text-to-image contrastive loss $L_{t \rightarrow i}$ is incorporated alongside $L_{i \rightarrow t}$, the resulting curves have no obvious changes. This empirical evidence strongly indicates that **the text-to-image contrastive loss has a limited ability to constrain modality alignment.**

Fig.12 (c, d) and (g, h) also present the changes in the CH index under different contrastive losses for LoRA-CLIP and MaPLE, respectively. It can be observed that the CH index of both visual and textual features is improved after using $L_{t \rightarrow i}$, and it can be further enhanced by using $L_{i \rightarrow t} + L_{t \rightarrow i}$. This suggests that **the role of the InfoNCE loss in CLIP is to strengthen the feature aggregation within the same class.**

D. Prompts for LLMs and Responses

D.1. Prompts for LLMs

To align with CLIP’s pre-training paradigm and enrich textual modality information [27], we employ Llama3-8B-Instruct [20] with 5 different LLM prompts to generate 10 class-specific descriptions per prompt, yielding a total of 50 semantically rich text descriptions per class. During the fine-tuning phase of each episode, we randomly select 30 descriptions per support set class as textual prompts. The class-wise mean of the resulting text features is computed and used as weights for the text classifier. The five distinct LLM prompts are as follows:

1. Describe what {article} {category} (a kind of {domain_word}) looks like in {max_len} words. Do not include any extra words or phrases.
2. How can you identify {article} {category} (a kind of {domain_word})? In {max_len} words.
3. Do not include any extra words or phrases. What are the identifying characteristics of {article} {category} (a kind of {domain_word}) in {max_len} words?
4. Do not include any extra words or phrases. What does {article} {category} (a kind of {domain_word}) look like? In {max_len} words. Do not include any extra words or phrases.

Table 5
Dataset Information

Dataset	Domain Description Word	(Partial) Category Names
CropDiseases	crop leaf	Apple__Apple_scab Blueberry__healthy Grape__Black_rot Tomato__Bacterial_spot Corn_(maize)__Northern_Leaf_Blight
EuroSAT	satellite image	Annual Crop Land, Sea or Lake, Forest, Herbaceous Vegetation Land, Highway or Road, Pasture Land, Industrial Buildings, Permanent Crop Land, River, Residential Buildings
ISIC	skin lesion image	Melanoma, Melanocytic Nevus, Basal, Cell Carcinoma, Benign Keratosis, Actinic Keratosis, Dermatofibroma
ChestX	diseased lung X-ray	Atelectasis, Cardiomegaly, Effusion, Infiltration, Mass, Nodule, Pneumothorax

5. Describe an image of {article} {category} (a kind of {domain_word}) in {max_len} words. Do not include any extra words or phrases.

where {category} represents the category name, {article} represents the article (a/an) chosen based on the category name, {domain_word} is the domain descriptor corresponding to the dataset, and {max_len} is used to control the length of the generated sentence to prevent exceeding the specified maximum token limit (77) of CLIP’s text encoder.

The specific domain description words and category names used in the prompts for different datasets are presented in Tab.5 .

D.2. Responses

Here we show two example responses of LLMs for a specific category within each dataset.

1. *Apple__Apple_scab* class in *CropDiseases*:

- A leaf with Apple Scab disease is typically yellow or pale green with large, circular, dark green or black lesions that are often surrounded by a yellow or white rim.
- Identify apple leaf with apple scab by observing: yellow-green, irregularly shaped spots with darker borders; powdery, white growth on underside; leaves may be distorted, curled, or crinkled; fungal odor; affected leaves often fall prematurely; can occur on both sides of leaf.

2. *Annual Crop Land* class in *EuroSAT*:

- A satellite image of annual crop land appears as a mosaic of rectangular fields with varying shades of green, often with narrow strips of darker or lighter tones indicating different crop types, irrigation patterns, and soil conditions.
- The image shows a vast expanse of green fields, rectangular in shape, with straight edges and

roads connecting them. The fields are divided into smaller sections, some with darker or lighter shades of green, indicating varying crop growth stages.

3. *Melanoma* class in *ISIC2018*:

- Irregularly shaped, dark brown or black mole with uneven borders, multiple colors, and diameter greater than 6 millimeters.
- Abnormal moles with asymmetry, irregular borders, varied colors, and diameter greater than 6mm.

4. *Atelectasis* class in *ChestX*:

- X-ray images of atelectasis show a collapsed lung with a dense, opaque appearance and loss of lung markings.
- Atelectasis appears as a dark or lucent area in the lung, often with a sharp border and surrounding hyperinflation.

E. Hyperparameter Analysis

We conduct a thorough analysis of the key hyperparameters in our proposed Semantic Probe framework to validate their influence on model performance. The parameters governing the Balanced Alignment and Separation (BAS) loss are the sigmoid steepness k , the decay threshold T , and the maximum initial value w , as defined in Eq. (13). For the EOS-guided Attention Rectification (EAR) module, the critical hyperparameter is the weighting coefficient α . Our analysis is performed on the 5-way 1-shot task, with results averaged across all four target datasets for clarity.

For the steepness parameter k , shown in Fig.13a, the average accuracy increases as k rises, indicating that a sharper transition from modality alignment to class separation is

Semantic Probe for SF-CDFSL

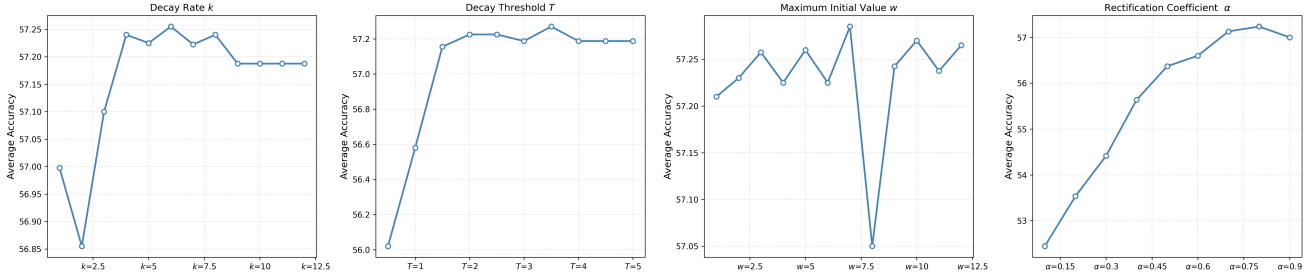


Figure 13: Performance of our Semantic Probe method under different configurations: (a) the steepness parameter k , (b) the decay threshold T , (c) the maximum initial value w , (d) the EOS-guided attention rectification weighting coefficient α .

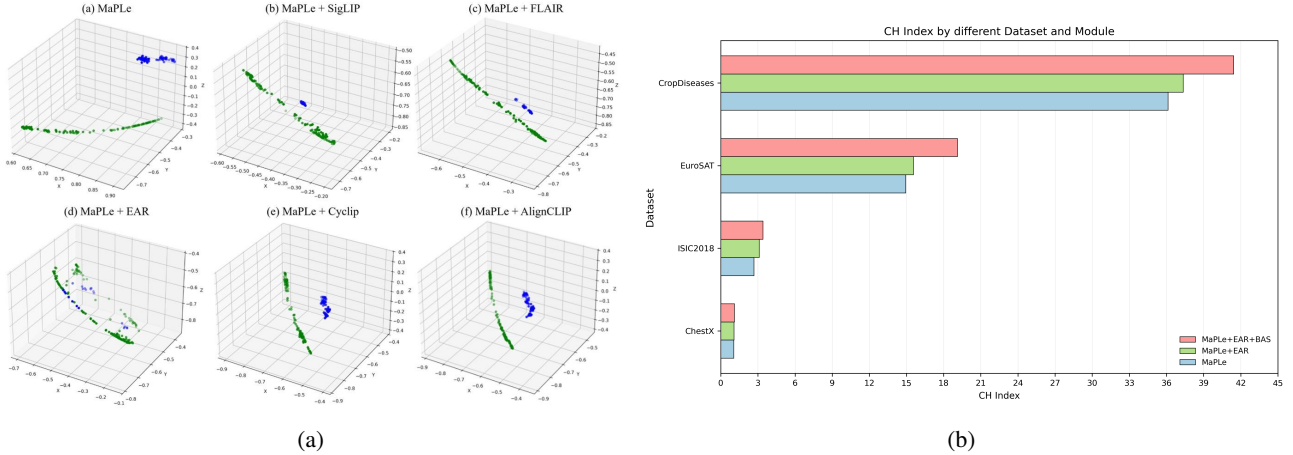


Figure 14: (a) DOSNES visualization of features under various CLIP-based methods. (b) The CH index of visual features across CDFSL target datasets.

generally beneficial. Performance then plateaus, demonstrating that the model is not overly sensitive to the exact value once an effective level of steepness is achieved. Fig.13b shows the impact of the threshold T , which dictates when the transition begins. Performance improves as the threshold increases, reaching its maximum at $T = 3.5$. A high threshold causes the model to pivot to class separation before modality alignment is sufficient, whereas a low threshold may delay this transition unnecessarily. The optimal value of $T = 3.5$ allows for a balanced training process. Fig.13c demonstrates the effect of the maximum initial value w . The average accuracy remains relatively stable across the tested range of w values, peaking at $w = 7$. This suggests that the model’s performance is robust to the initial weighting of the alignment loss, as long as it provides sufficient guidance without dominating the total loss.

The weighting coefficient α (defined in Eq. (9)) in the EAR module determines the balance between the original CLS token’s attention and the textual EOS token’s guidance. As shown in Figure 13d, when α is low (e.g., 0.1), the influence of the original CLS attention is too small, resulting in suboptimal performance. As we increase α , performance improves significantly, as the model effectively integrates the guided attention with its own learned patterns. The performance peaks at $\alpha = 0.8$, demonstrating that a enough but not overwhelming influence from the textual modality is most effective.

F. Layer placement of the EAR module

EAR is only applied to the final layers of CLIP. This design choice was motivated by prior work, particularly MMA [37] and MMRL [8], which established two key findings:

- Deep layers encode task-specific discriminative knowledge for fine-tuning; shallow layers preserve universal cross-domain knowledge and should be frozen.
- Textual features are more discriminative than visual features, and the semantic gap between modalities is larger at shallow layers, making cross-modal alignment more challenging.

Additional layer experiments (5-way 1-shot) are shown in Table 6. Deep-layer placement yields the best performance across all datasets, consistent with the above analysis.

G. Comparison with CLIP-based Methods

We further extend our comparative analysis to include other prominent CLIP-based methods, namely SigLIP [41], FLAIR [34], CyCLIP [6], and AlignCLIP [3]. Their 5-shot classification accuracy, evaluated on the MaPLc baseline, is presented in Table 7. It is noteworthy that, given the many-to-one relationship between images and texts in CDFSL

Table 6

Ablation study on different layer groups for the 5-way 1-shot classification task.

Layers	Ches.	ISIC.	Euro.	Crop.	Ave.
1-4	21.86	39.25	82.37	84.44	56.98
5-8	21.95	39.95	82.57	84.76	57.31
9-12	22.34	39.96	83.24	84.82	57.39

Table 7

Comparison with CLIP-based works by the 5-way 5-shot classification on MaPLe.

Method	ChestX	ISIC	EuroSAT	CropDiseases	Ave.
MaPLe	23.62	49.02	89.58	93.00	63.81
MaPLe + SigLIP	20.08	22.79	61.87	54.32	39.77
MaPLe + FLAIR	20.07	22.77	61.84	54.30	39.75
MaPLe + CyCLIP	24.40	51.58	92.06	94.19	65.56
MaPLe + AlignCLIP	24.19	51.78	91.78	94.20	65.49
MaPLe + Ours	24.86	53.11	92.50	94.85	66.33

tasks, both CyCLIP and AlignCLIP adapt their approach by replacing intra-batch image-text features with modal category mean features. Despite these specialized adaptations, our proposed method consistently achieves optimal performance.

H. Module Verification

Fig.14a illustrates the feature distributions of visual and textual modalities for various CLIP-based methods using DOSNES [21] visualization. Initially, MaPLe exhibits a distinct separation between visual and textual features. While methods such as SigLIP, FLAIR, CyCLIP, and AlignCLIP reduce the center distance between modalities, they fail to effectively achieve feature fusion. In contrast, MaPLe with our EAR significantly enhances modality integration.

Fig.14b reports the Calinski-Harabasz (CH) index for visual features across three configurations: MaPLe, MaPLe with EAR, and MaPLe with EAR + BAS. The results indicate that: (1) EAR strengthens class separation within the visual modality; and (2) when combined with BAS, the class separation is further improved due to enhanced modality alignment. These findings confirm that improved modality alignment fosters better class separation, a critical factor for superior CDFSL performance.

I. Comparison with SOTA CDFSL Methods

Tables 8 and 9 provide a comprehensive comparison of our proposed Semantic Probe framework with state-of-the-art approaches, including MEM-FS [31], StyleAdv [4], FLoR [47], DAMIM [22], AttnTemp [48], CD-CLS [49], PMF [11], IM-DCL [35], and StepSPT [36], for 5-way 1-shot and 5-shot classification tasks. These methods employ varied backbones and training configurations, differing in whether they utilize source domain pre-training (e.g., mini-ImageNet) or target domain fine-tuning (FT). Our method, specifically LoRA-CLIP + Ours, achieves the highest average performance of 57.62% in the 1-shot setting and 68.01% in the 5-shot setting, outperforming all competitors.

It is noteworthy that IM-DCL [35] achieves superior performance on the ChestX dataset, which we attribute to its ResNet-based backbone being better suited for capturing local features prevalent in medical images.

CRedit authorship contribution statement

Yaze Zhao: Writing – review and editing, Writing – original draft, Visualization, Validation, Methodology, Investigation, Formal analysis, Data curation, Conceptualization. **Yicong Liu:** Writing – review and editing, Writing – original draft, Visualization, Validation, Methodology, Investigation, Formal analysis, Data curation, Conceptualization. **Yixiong Zou:** Writing – review and editing, Supervision, Methodology, Funding acquisition. **Yuhua Li:** Resources, Project administration. **Ruixuan Li:** Resources, Project administration.

Declaration of competing interest

I confirm that no authors of this manuscript have any competing financial or non-financial interests, currently or previously, including serving in an editorial capacity for the journal we are submitting to.

Acknowledgments

This work is supported by the National Natural Science Foundation of China under grants 62206102; the National Key Research and Development Program of China under grant 2024YFC3307900; the National Natural Science Foundation of China under grants 62436003, 62376103 and 62302184; Major Science and Technology Project of Hubei Province under grant 2025BAB011 and 2024BAA008; Hubei Science and Technology Talent Service Project under grant 2024DJC078; and Ant Group through CCF-Ant Research Fund. The computation is completed in the HPC Platform of Huazhong University of Science and Technology.

References

- [1] Codella, N., Rotemberg, V., Tschandl, P., Celebi, M.E., Dusza, S., Gutman, D., Helba, B., Kalloo, A., Liopyris, K., Marchetti, M., et al., 2019. Skin lesion analysis toward melanoma detection 2018: A challenge hosted by the international skin imaging collaboration (isic). arXiv preprint arXiv:1902.03368.
- [2] Dosovitskiy, A., Beyer, L., Kolesnikov, A., Weissenborn, D., Zhai, X., Unterthiner, T., Dehghani, M., Minderer, M., Heigold, G., Gelly, S., Uszkoreit, J., Houlsby, N., 2021. An image is worth 16x16 words: Transformers for image recognition at scale, in: ICLR 2021.
- [3] Eslami, S., de Melo, G., 2024. Mitigate the gap: Investigating approaches for improving cross-modal alignment in clip. arXiv preprint arXiv:2406.17639.
- [4] Fu, Y., Xie, Y., Fu, Y., Jiang, Y., 2023. Styleadv: Meta style adversarial training for cross-domain few-shot learning, in: IEEE/CVF Conference on Computer Vision and Pattern Recognition, CVPR 2023, Vancouver, BC, Canada, June 17-24, 2023, IEEE. pp. 24575–24584.
- [5] Gao, P., Geng, S., Zhang, R., Ma, T., Fang, R., Zhang, Y., Li, H., Qiao, Y., 2024. Clip-adapter: Better vision-language models with feature adapters. International Journal of Computer Vision 132, 581–595.

Table 8

Comparison with state-of-the-art works by the 5-way 1-shot classification.

Method	Backbone	Mark	Source	Target	ChestX	ISIC	EuroSAT	CropDiseases	Ave.
MEM-FS	ViT/DINO	TIP-23			22.76	32.97	68.11	81.11	51.24
StyleAdv	ViT/DINO	CVPR-23	✓	-	22.92	33.05	72.15	81.22	52.34
FLoR	ViT/DINO	CVPR-24	✓	-	22.78	34.20	72.39	81.81	52.80
DAMIM	ViT/DINO	AAAI-25	✓	-	22.97	34.66	72.87	82.34	53.21
AttnTemp	ViT/DINO	NeurIPS-24	✓	-	23.19	34.92	74.35	84.02	54.12
CD-CLS	ViT/DINO	NeurIPS-24	✓	✓	23.39	35.56	74.97	84.53	54.62
PMF	ViT/DINO	CVPR-22	✓	✓	21.73	30.36	70.74	80.79	50.91
StyleAdv-FT	ViT/DINO	CVPR-23	✓	✓	22.92	33.99	74.93	84.11	53.99
FLoR-FT	ViT/DINO	CVPR-24	✓	✓	23.26	35.49	73.09	83.55	53.85
DAMIN-FT	ViT/DINO	AAAI-25	✓	✓	23.38	36.35	73.61	83.90	54.31
AttnTemp-FT	ViT/DINO	NeurIPS-24	✓	✓	23.63	38.05	75.09	84.78	55.39
IM-DCL	RN10	TIP-24	-	✓	23.98	38.13	77.14	84.37	55.91
StepSPT	ViT/CLIP	TPAMI-25	-	✓	22.84	32.97	70.01	84.84	52.68
MaPLe	ViT/CLIP	CVPR-23	-	✓	20.89	31.10	75.66	81.87	53.04
MaPLe + Ours	ViT/CLIP	-	-	✓	21.41	34.27	82.94	82.83	55.36
Δ	-	-	-	-	+0.52	+3.17	+7.28	+0.96	+2.32
LoRA-CLIP	ViT/CLIP	CVPR-24	-	✓	21.73	34.45	80.34	84.95	55.37
LoRA-CLIP + Ours	ViT/CLIP	-	-	✓	23.65	38.77	82.94	85.11	57.62
Δ	-	-	-	-	+1.92	+4.43	+2.60	+0.16	+2.25

Table 9

Comparison with state-of-the-art works by the 5-way 5-shot classification.

Method	Backbone	Mark	Source	Target	ChestX	ISIC	EuroSAT	CropDiseases	Ave.
MEM-FS	ViT/DINO	TIP-23			26.67	47.38	86.49	93.74	63.57
StyleAdv	ViT/DINO	CVPR-23	✓	-	26.97	47.73	88.57	94.85	64.53
FLoR	ViT/DINO	CVPR-24	✓	-	27.28	49.52	90.41	95.28	65.48
DAMIM	ViT/DINO	AAAI-25	✓	-	27.28	50.76	89.50	95.52	65.77
AttnTemp	ViT/DINO	NeurIPS-24	✓	-	27.72	53.09	90.13	95.53	66.62
CD-CLS	ViT/DINO	NeurIPS-24	✓	✓	27.66	54.69	91.53	96.27	67.54
PMF	ViT/DINO	CVPR-22	✓	✓	27.27	50.12	85.98	92.96	64.08
StyleAdv-FT	ViT/DINO	CVPR-23	✓	✓	26.97	51.23	90.12	95.99	66.08
FLoR-FT	ViT/DINO	CVPR-24	✓	✓	27.02	53.06	90.75	96.47	66.83
DAMIN-FT	ViT/DINO	AAAI-25	✓	✓	27.82	54.86	91.18	96.34	67.78
AttnTemp-FT	ViT/DINO	NeurIPS-24	✓	✓	28.03	54.91	90.82	96.66	67.61
IM-DCL	RN10	TIP-24	-	✓	28.93	52.74	89.47	95.73	66.72
StepSPT	ViT/CLIP	TPAMI-25	-	✓	26.36	52.12	89.40	96.01	65.97
MaPLe	ViT/CLIP	CVPR-23	-	✓	22.29	46.72	88.82	93.15	62.75
MaPLe + Ours	ViT/CLIP	-	-	✓	24.86	53.11	92.50	94.85	66.33
Δ	-	-	-	-	+2.57	+6.39	+3.68	+1.70	+3.58
LoRA-CLIP	ViT/CLIP	CVPR-24	-	✓	24.44	50.68	92.63	96.20	65.99
LoRA-CLIP + Ours	ViT/CLIP	-	-	✓	25.79	55.95	93.43	96.88	68.01
Δ	-	-	-	-	+1.35	+5.27	+0.80	+0.48	+2.02

- [6] Goel, S., Bansal, H., Bhatia, S., Rossi, R., Vinay, V., Grover, A., 2022. Cyclip: Cyclic contrastive language-image pretraining. *Advances in Neural Information Processing Systems* 35, 6704–6719.
- [7] Guo, Y., Codella, N.C., Karlinsky, L., Codella, J.V., Smith, J.R., Saenko, K., Rosing, T., Feris, R., 2020. A broader study of cross-domain few-shot learning, in: *Computer vision—ECCV 2020: 16th European conference, glasgow, UK, August 23–28, 2020, proceedings, part XXVII 16*, Springer. pp. 124–141.
- [8] Guo, Y., Gu, X., 2025. MMRL: multi-modal representation learning for vision-language models, in: *IEEE/CVF Conference on Computer Vision and Pattern Recognition, CVPR 2025, Nashville, TN, USA, June 11–15, 2025*, Computer Vision Foundation / IEEE. pp. 25015–25025.
- [9] Helber, P., Bischke, B., Dengel, A., Borth, D., 2019. Eurosat: A novel dataset and deep learning benchmark for land use and land cover classification. *IEEE Journal of Selected Topics in Applied Earth Observations and Remote Sensing* 12, 2217–2226.
- [10] Hu, E.J., Shen, Y., Wallis, P., Allen-Zhu, Z., Li, Y., Wang, S., Wang, L., Chen, W., 2022a. Lora: Low-rank adaptation of large language models, in: *The Tenth International Conference on Learning Representations, ICLR 2022, Virtual Event, April 25–29, 2022*, OpenReview.net.
- [11] Hu, S.X., Li, D., Stühmer, J., Kim, M., Hospedales, T.M., 2022b. Pushing the limits of simple pipelines for few-shot learning: External data and fine-tuning make a difference, in: *CVPR 2022, IEEE*. pp. 9058–9067.
- [12] Hu, Z., Wang, L., Lan, Y., Xu, W., Lim, E., Bing, L., Xu, X., Poria, S., Lee, R.K., 2023. Llm-adapters: An adapter family for parameter-efficient fine-tuning of large language models, in: Bouamor, H., Pino, J., Bali, K. (Eds.), *Proceedings of the 2023 Conference on Empirical Methods in Natural Language Processing, EMNLP 2023, Singapore, December 6–10, 2023*, Association for Computational Linguistics. pp. 5254–5276.
- [13] Huang, Y., Shakeri, F., Dolz, J., Boudiaf, M., Bahig, H., Ayed, I.B., 2024. Lp++: A surprisingly strong linear probe for few-shot clip, in: *IEEE/CVF Conference on Computer Vision and Pattern Recognition (CVPR)*.
- [14] Jia, M., Tang, L., Chen, B.C., Cardie, C., Belongie, S., Hariharan, B., Lim, S.N., 2022. Visual prompt tuning, in: *European conference on computer vision, Springer*. pp. 709–727.

- [15] Khattak, M.U., Rasheed, H., Maaz, M., Khan, S., Khan, F.S., 2023a. Maple: Multi-modal prompt learning, in: Proceedings of the IEEE/CVF conference on computer vision and pattern recognition, pp. 19113–19122.
- [16] Khattak, M.U., Wasim, S.T., Naseer, M., Khan, S., Yang, M., Khan, F.S., 2023b. Self-regulating prompts: Foundational model adaptation without forgetting, in: IEEE/CVF International Conference on Computer Vision, ICCV 2023, Paris, France, October 1-6, 2023, IEEE. pp. 15144–15154.
- [17] Li, S., Liu, F., Hao, Z., Wang, X., Li, L., Liu, X., Chen, P., Ma, W., 2025. Logits deconfusion with clip for few-shot learning, in: Proceedings of the Computer Vision and Pattern Recognition Conference (CVPR), pp. 25411–25421.
- [18] Liang, H., Zhang, Q., Dai, P., Lu, J., 2021. Boosting the generalization capability in cross-domain few-shot learning via noise-enhanced supervised autoencoder, in: Proceedings of the IEEE/CVF international conference on computer vision, pp. 9424–9434.
- [19] Liang, V.W., Zhang, Y., Kwon, Y., Yeung, S., Zou, J.Y., 2022. Mind the gap: Understanding the modality gap in multi-modal contrastive representation learning. *Advances in Neural Information Processing Systems* 35, 17612–17625.
- [20] Llama Team, 2024. The llama 3 herd of models. arXiv preprint arXiv:2407.21783. URL: <https://arxiv.org/abs/2407.21783>, doi:10.48550/arXiv.2407.21783.
- [21] Lu, Y., Corander, J., Yang, Z., 2016. Doubly stochastic neighbor embedding on spheres. arXiv preprint arXiv:1609.01977.
- [22] Ma, R., Zou, Y., Li, Y., Li, R., 2025. Reconstruction target matters in masked image modeling for cross-domain few-shot learning, in: Walsh, T., Shah, J., Kolter, Z. (Eds.), AAAI-25, Sponsored by the Association for the Advancement of Artificial Intelligence, February 25 - March 4, 2025, Philadelphia, PA, USA, AAAI Press. pp. 19305–19313.
- [23] Mohanty, S.P., Hughes, D.P., Salathé, M., 2016. Using deep learning for image-based plant disease detection. *Frontiers in plant science* 7, 215232.
- [24] van den Oord, A., Li, Y., Vinyals, O., 2018. Representation learning with contrastive predictive coding. arXiv preprint arXiv:1807.03748. URL: <https://arxiv.org/abs/1807.03748>.
- [25] Pratt, S.M., Covert, I., Liu, R., Farhadi, A., 2023. What does a platypus look like? generating customized prompts for zero-shot image classification, in: IEEE/CVF International Conference on Computer Vision, ICCV 2023, Paris, France, October 1-6, 2023, IEEE. pp. 15645–15655.
- [26] Radford, A., Kim, J.W., Hallacy, C., Ramesh, A., Goh, G., Agarwal, S., Sastry, G., Askell, A., Mishkin, P., Clark, J., et al., 2021. Learning transferable visual models from natural language supervision, in: International conference on machine learning, PmlR. pp. 8748–8763.
- [27] Schrodi, S., Hoffmann, D.T., Argus, M., Fischer, V., Brox, T., 2024. Two effects, one trigger: on the modality gap, object bias, and information imbalance in contrastive vision-language representation learning. arXiv preprint arXiv:2404.07983.
- [28] Tang, Y., Lin, Z., Wang, Q., Zhu, P., Hu, Q., 2024. Amu-tuning: Effective logit bias for clip-based few-shot learning, in: IEEE/CVF Conference on Computer Vision and Pattern Recognition, CVPR 2024, Seattle, WA, USA, June 16-22, 2024, IEEE. pp. 23323–23333.
- [29] Tseng, H.Y., Lee, H.Y., Huang, J.B., Yang, M.H., 2020. Cross-domain few-shot classification via learned feature-wise transformation. arXiv preprint arXiv:2001.08735.
- [30] Tyshchuk, K., Karpikova, P., Spiridonov, A., Prutianova, A., Razzhigaev, A., Panchenko, A., 2023. On isotropy of multimodal embeddings. *Information* 14, 392.
- [31] Walsh, R., Osman, I.I., Shehata, M.S., 2023. Masked embedding modeling with rapid domain adjustment for few-shot image classification. *IEEE Trans. Image Process.* , 4907–4920.
- [32] Wang, H., Deng, Z.H., 2021. Cross-domain few-shot classification via adversarial task augmentation. arXiv preprint arXiv:2104.14385.
- [33] Wang, X., Peng, Y., Lu, L., Lu, Z., Bagheri, M., Summers, R.M., 2017. Chestx-ray8: Hospital-scale chest x-ray database and benchmarks on weakly-supervised classification and localization of common thorax diseases, in: 2017 IEEE Conference on Computer Vision and Pattern Recognition, CVPR 2017, Honolulu, HI, USA, July 21-26, 2017, IEEE Computer Society. pp. 3462–3471.
- [34] Xiao, R., Kim, S., Georgescu, M.I., Akata, Z., Alaniz, S., 2024. Flair: Vlm with fine-grained language-informed image representations. arXiv preprint arXiv:2412.03561.
- [35] Xu, H., Liu, L., Zhi, S., Fu, S., Su, Z., Cheng, M., Liu, Y., 2024a. Enhancing information maximization with distance-aware contrastive learning for source-free cross-domain few-shot learning. *IEEE Trans. Image Process.* , 2058–2073.
- [36] Xu, H., Liu, Y., Liu, L., Zhi, S., Sun, S., Liu, T., Cheng, M.M., 2024b. Step-wise distribution alignment guided style prompt tuning for source-free cross-domain few-shot learning. arXiv preprint arXiv:2411.10070. URL: <https://arxiv.org/abs/2411.10070>.
- [37] Yang, L., Zhang, R.Y., Wang, Y., Xie, X., 2024. Mma: Multi-modal adapter for vision-language models, in: Proceedings of the IEEE/CVF Conference on Computer Vision and Pattern Recognition (CVPR), pp. 23826–23837.
- [38] Yang, Y., Deng, J., Li, W., Duan, L., 2025. Resclip: Residual attention for training-free dense vision-language inference, in: IEEE/CVF Conference on Computer Vision and Pattern Recognition, CVPR 2025, Nashville, TN, USA, June 11-15, 2025, Computer Vision Foundation / IEEE. pp. 29968–29978.
- [39] Yazdanpanah, M., Moradi, P., 2022. Visual domain bridge: A source-free domain adaptation for cross-domain few-shot learning, in: IEEE/CVF Conference on Computer Vision and Pattern Recognition Workshops, CVPR Workshops 2022, New Orleans, LA, USA, June 19-20, 2022, IEEE. pp. 2867–2876. URL: <https://doi.org/10.1109/CVPRW56347.2022.00324>, doi:10.1109/CVPRW56347.2022.00324.
- [40] Zanella, M., Ayed, I.B., 2024. Low-rank few-shot adaptation of vision-language models, in: IEEE/CVF Conference on Computer Vision and Pattern Recognition, CVPR 2024 - Workshops, Seattle, WA, USA, June 17-18, 2024, IEEE. pp. 1593–1603.
- [41] Zhai, X., Mustafa, B., Kolesnikov, A., Beyer, L., 2023. Sigmoid loss for language image pre-training, in: Proceedings of the IEEE/CVF international conference on computer vision, pp. 11975–11986.
- [42] Zhang, R., Fang, R., Zhang, W., Gao, P., Li, K., Dai, J., Qiao, Y., Li, H., 2021. Tip-adapter: Training-free clip-adapter for better vision-language modeling. arXiv preprint arXiv:2111.03930.
- [43] Zhang, R., Zhang, W., Fang, R., Gao, P., Li, K., Dai, J., Qiao, Y., Li, H., 2022. Tip-adapter: Training-free adaption of CLIP for few-shot classification, in: Computer Vision - ECCV 2022 - 17th European Conference, pp. 493–510.
- [44] Zhou, F., Wang, P., Zhang, L., Wei, W., Zhang, Y., 2023. Revisiting prototypical network for cross domain few-shot learning, in: Proceedings of the IEEE/CVF conference on computer vision and pattern recognition, pp. 20061–20070.
- [45] Zhou, K., Yang, J., Loy, C.C., Liu, Z., 2022. Learning to prompt for vision-language models. *International Journal of Computer Vision* 130, 2337–2348.
- [46] Zhuo, L., Wang, Z., Fu, Y., Qian, T., 2024. Prompt as free lunch: Enhancing diversity in source-free cross-domain few-shot learning through semantic-guided prompting. arXiv preprint arXiv:2412.00767. URL: <https://arxiv.org/abs/2412.00767>.
- [47] Zou, Y., Liu, Y., Hu, Y., Li, Y., Li, R., 2024a. Flatten long-range loss landscapes for cross-domain few-shot learning, in: CVPR 2024, IEEE. pp. 23575–23584.
- [48] Zou, Y., Ma, R., Li, Y., Li, R., 2024b. Attention temperature matters in vit-based cross-domain few-shot learning. *Advances in Neural Information Processing Systems* 37, 116332–116354.
- [49] Zou, Y., Yi, S., Li, Y., Li, R., 2024c. A closer look at the CLS token for cross-domain few-shot learning, in: NeurIPS 2024.



Yaze Zhao received the B.S. degree from the School of Computer Science and Technology, Huazhong University of Science and Technology, Wuhan, China. He is also pursuing the master's degree at the School of Computer Science and Technology, Huazhong University of Science and Technology. His primary research interests include few-shot learning, domain adaptation, and multimodal models.



Yicong Liu received the B.S. degree from the College of Computer Science and Electronic Engineering, Hunan University. She received the M.S. degree from the School of Computer Science and Technology, Huazhong University of Science and Technology. Her primary research interests include few-shot learning and frequency domain analysis.



Yixiong Zou received the B.S. degree from Nankai University, and received the Ph.D. degree from the School of Electrical Engineering and Computer Science, Peking University, Beijing, China. He was a visiting scholar at Carnegie Mellon University. He has published more than 40 journal and conference papers. He is currently a Lecturer with the School of Computer Science and Technology, Huazhong University of Science and Technology. His research interests include multimodal large language models, few-shot learning, open-world learning, and computer vision.



Yuhua Li received the Ph.D. degree in computer application technology from Huazhong University of Science and Technology, Wuhan, China, in 2006. She is currently a Professor in the School of Computer Science and Technology, Huazhong University of Science and Technology. She was a visiting scholar at the University of California, Santa Barbara. She has published more than 60 journal and conference papers (NeurIPS, TKDE, SIGIR, WWW, ICDM, IJCAI). She is also a senior member of the China Computer Federation (CCF). Her research interests include data mining, social networks, machine learning, and big data.



Ruixuan Li received the B.S., M.S., and Ph.D. degrees in computer science from the Huazhong University of Science and Technology in 1997, 2000, and 2004, respectively. From 2009 to 2010, he was a Visiting Researcher with the Department of Electrical and Computer Engineering, University of Toronto. He is currently a Professor with the School of Computer Science and Technology, Huazhong University of Science and Technology. His research interests include cloud and edge computing, big data management, and distributed system security. He has published more than 500 journal and conference papers (NeurIPS, KDD, ICDM, IJCAI). He is also a member of ACM.